



24 **Abstract**

25 Introduction

26 Clinical tools are neither standardized nor ubiquitous to monitor volumetric or morphological  
27 changes in the periorbital region and ocular adnexa due to pathology such as oculofacial trauma,  
28 thyroid eye disease, and the natural aging process. We have developed a low-cost, three  
29 dimensionally printed **PH**otogrammetry for **A**utomated **CarE** (PHACE) system to evaluate three-  
30 dimensional (3D) measurements of periocular and adnexal tissue.

31

32 Methods

33 The PHACE system uses two Google Pixel 3 smartphones attached to automatic rotating  
34 platforms to image a subject's face through a cutout board patterned with registration marks.  
35 Photographs of faces were taken from many perspectives by the cameras placed on the rotating  
36 platform. Faces were imaged with and without 3D printed hemispheric phantom lesions (black  
37 domes) affixed on the forehead above the brow. Images were rendered into 3D models in  
38 Metashape (Agisoft, St. Petersburg, Russia) and then processed and analyzed in CloudCompare  
39 (CC) and Autodesk's Meshmixer. The 3D printed hemispheres affixed to the face were then  
40 quantified within Meshmixer and compared to their known volumes. Finally, we compared  
41 digital exophthalmometry measurements with results from a standard Hertel exophthalmometer  
42 in a subject with and without an orbital prosthesis.

43

44 Results

45 Quantification of 3D printed phantom volumes using optimized stereophotogrammetry  
46 demonstrated a 2.5% error for a 244 $\mu$ L phantom, and 7.6% error for a 27.5 $\mu$ L phantom. Digital  
47 exophthalmometry measurements differed by 0.72mm from a standard exophthalmometer.

48

49 Conclusion

50 We demonstrated an optimized workflow using our custom apparatus to analyze and quantify  
51 oculofacial volumetric and dimensions changes with a resolution of 244 $\mu$ L. This apparatus is a  
52 low-cost tool that can be used in clinical settings to objectively monitor volumetric and  
53 morphological changes in periorbital anatomy.

## 54 **Introduction**

55           Photogrammetry is the science of calculating spatial and geometric information from  
56 objects based on their photographs.<sup>1</sup> This technology was traditionally used in the fields of  
57 cartography and geodesy in conjunction with the advent of photography in the 19<sup>th</sup> century.  
58 Modern improvements in the portability, resolution, cost of image capture, and advancements in  
59 the sophistication of computer software have led to adoption of photogrammetry across many  
60 disciplines.<sup>2,3</sup> In medicine, photogrammetry can offer objective measurements of body  
61 anthropometry that may be useful in assessing growth and development, treatment response, and  
62 surgical outcomes.<sup>4-7</sup>

63           In ophthalmology, two-dimensional (2D) photographs have long been used for assessment  
64 of clinical and surgical outcomes. Examples of 2D photography in ophthalmology include pre-  
65 and post-operative comparisons in oculoplastic surgery, monitoring of the anterior segment angle  
66 anatomy, and evaluation of optic nerve fiber anatomy.<sup>8-11</sup> Gradual introduction of three-  
67 dimensional (3D) external anatomy imaging technologies over the past decade achieve shorter  
68 acquisition times, higher safety, cost-effectiveness, and greater ease of use.<sup>12,13</sup>

69           The two most common classes of 3D facial surface imaging technologies include structured  
70 light technology and stereophotogrammetry. Structured light scanners are considered “active”  
71 because they emit grid patterns of visible or infrared light over an object’s surface. 3D shapes are  
72 generated by analyzing and calculating distortions in the projected grid as it optically conforms to  
73 the scanned object’s contour.<sup>14</sup> Stereophotogrammetry scanners are considered “passive” because  
74 imaging is performed without projecting light patterns onto the scanned object. Photographs of an  
75 object are taken from multiple angles to acquire different surface perspectives, which are used to  
76 calculate relative spatial coordinates and geometry in 3D space.<sup>13-15</sup>

77 Hybrid scanners that utilize both structured light and stereophotogrammetry (i.e., active  
78 stereophotogrammetry) have become available for medical use in recent years. The suite of 3dMD  
79 products (3dMD, Atlanta, GA) are an example of large, multi-camera setups that simultaneously  
80 capture images from multiple angles and additionally use structured light. A number of studies  
81 have independently verified their high degree of accuracy and reliability.<sup>16-19</sup> However, due to the  
82 high cost, limited portability, and need for frequent recalibration of these 3dMD products, a  
83 number of companies have developed handheld, single lens reflex device alternatives such as the  
84 Vectra H2 (Canfield Scientific Inc., Fairfield, NJ) and Artec Eva (Artec, Luxembourg).<sup>20,21</sup> These  
85 devices benefit from a high degree of portability and lower cost at the expense of accuracy given  
86 the sequential capture method. Despite the decreased accuracy, comparison studies have shown  
87 sufficient accuracy for use in many clinical applications.<sup>12, 21-24</sup> Still, these handheld devices cost  
88 thousands of dollars, which may preclude their widespread adoption in general clinical practice.  
89 To address the cost concern, Rudy et al. demonstrated the feasibility of using the iPhone X (Apple,  
90 Inc., Cupertino, CA) for 3D facial capture in the setting of plastic surgery.<sup>25</sup> A breakdown of costs,  
91 3D scanning method, and relative accuracies for each of the available devices on the market are  
92 summarized in Table 1.

93

94 Table 1. Stereophotogrammetry devices currently available on the market.<sup>26-29</sup>

Product Name	Cost	3D Scanning Method	Relative Accuracy
3dMD face	\$10000	Active stereophotogrammetry	0.2mm
Vectra H2	\$8000	Stereophotogrammetry	1.2mm
Artec Eva	\$19800	Structured-light 3D scanner	0.1mm
iPhone X (refurb)	\$200	Active stereophotogrammetry	1mm

95

96           3D imaging devices, including the 3dMD and Vectra M3 systems are suitable for  
97 characterizing the periocular region.<sup>30-33</sup> However, to the best of our knowledge, no studies have  
98 investigated the optimization and use of low-cost photogrammetry systems for periocular  
99 applications. The purpose of this study was to optimize and evaluate a low-cost (<\$300 USD), 3D  
100 printed photogrammetry acquisition system for quantitative analysis of periorbital and ocular  
101 adnexa morphology and volumetry.

102

## 103 **Methods**

### 104 *Study Design*

105           This study received Institutional Review Board approval from the University of California,  
106 Irvine and was conducted in accordance with the Declaration of Helsinki. Due to limitations of the  
107 approved IRB, only portions of faces are shown. Studies performed were HIPAA-compliant and  
108 all enrolled participants provided written informed consent.

109           In this study, a novel data capture system and manual analysis protocol called  
110 PHotogrammetry for Automated CarE (PHACE) was evaluated for dimensional accuracy and  
111 precision by comparing 3D rendered facial models to real world measurements. This study  
112 included 15 healthy adults between the ages of 20 and 65 years (mean age  $40 \pm 20$  years). There  
113 were 9 males and 6 females with Fitzpatrick skin types 2, 4, and 6. We evaluated how the number  
114 of images from different angles impact 3D model quality when models were generated using  
115 several different photogrammetry software tools. We further assessed the precision and accuracy  
116 of rendered models by performing depth and volumetric analysis of phantom lesions placed on

117 human subjects. Lastly, the PHACE system was evaluated in an anophthalmic male between 35-  
118 40 year-old with Fitzpatrick skin type 2 with and without his left ocular prosthetic.

119

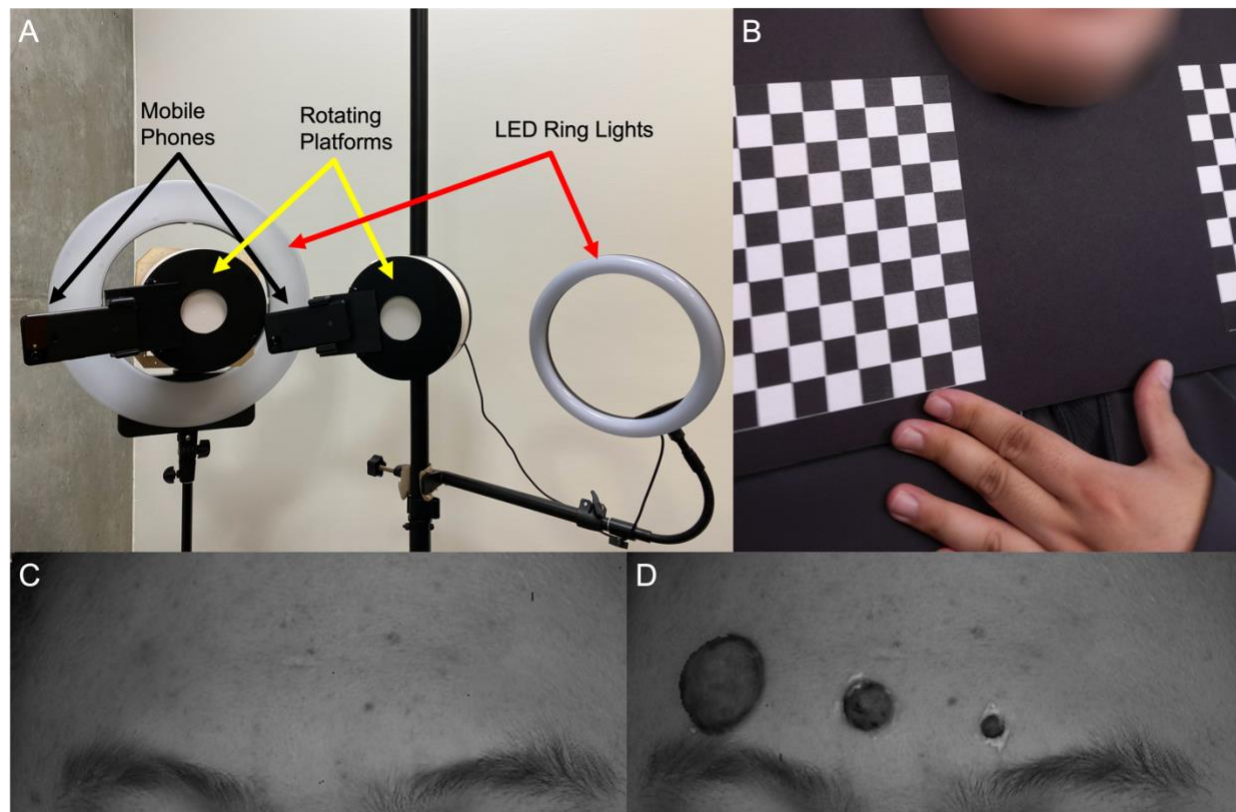
### 120 *Imaging System*

121 The imaging system utilizes two off-the-shelf motorized turntables modified with custom  
122 designed 3D printed phone mounts 1.5ft from the platform base and 1.25ft from each other. Each  
123 rotation device was clamped onto height adjustable stands with illumination ring lights. Each ring  
124 light was set to a brightness of 24,000 lux and 4400K color temperature.

125 Images were acquired using two Google Pixel 3 smartphones (Android 11 operating  
126 system) using the Manual Camera app (Lenses Inc.). User-defined camera settings included: ISO  
127 55, shutter speed 1/80 seconds, focal distance 0.46m (1.5ft), 8MP resolution, portrait orientation  
128 lock, and automatic repeating shutter at an acquisition rate of 1 photo/second.

129 Each smartphone camera was positioned 45cm from the subjects' glabella with the  
130 rotational axis between phones being 38cm apart at the base. The minimum and maximum  
131 vergence angles were 0° and 140.8°. The axis of rotation for each smartphone-rotation device was  
132 centered on the face. Subjects placed their faces through a foam board cutout with checker patterns  
133 for image registration (Figure 1-A). Subjects were instructed to remain motionless with a relaxed  
134 facial expression and closed eyes. Pictures of the phantom lesions and the anophthalmic human  
135 subject were taken at a rate of one photograph/second and a total of 90 images were processed per  
136 subject.

137



138

139

140

141

142

Figure 1. A) Photogrammetry apparatus with two smartphones attached to rotating platforms illuminated by 2 ring LED lights. B) Subjects place their faces through a backdrop with reference checkered squares. Rendered faces without domes (C) and with domes (D).

*\*Pictures have been modified to adhere to Medrxiv picture policy. Please contact corresponding author to request access to this material.*

### Generating 3D Models

143

144

145

146

147

148

Photographs were rendered as 3D facial models and analyzed on a Gigabyte Z390 Aorus Ultra Gaming PC running Windows 10 with an Intel Core i9-9900k 8-core CPU @ 3.6GHz, 48GB of RAM, and a Nvidia GeForce RTX 2080 graphics card. After photographs were taken, a custom python script split RGB images into red, green, and blue channels. Blue channel photos were then imported into four photogrammetry software programs and the quality of rendered models was evaluated using Autodesk's 3D modeling software.



149           The four different photogrammetry software tools evaluated were Metashape (Agisoft, St.  
150 Petersburg, Russia), Meshroom (AliceVision, Open-source), Pix4Dcloud (Pix4D S.A., Prilly  
151 Switzerland), and Zephyr3D (3DFLOW, Verona, Italy). The data set used for comparing  
152 photogrammetry software utilized the same set of 90 photographs. Each software was set to the  
153 highest settings for alignment, point cloud generation, and mesh rendering. Models from each  
154 photogrammetry software were exported as a wavefront object file (.obj file) and then imported  
155 into Autodesk's Meshmixer 3D modeling software for scaling and comparison analysis. The  
156 overall quality of rendered models from each photogrammetry software was visually evaluated.  
157 Accuracy and precision were qualitatively evaluated by assessing how similar 3D models  
158 resembled the human subject face using two metrics: facial shape and surface texture (smooth or  
159 rough).

160           The relationship between the number of images required to be processed without a loss of  
161 model precision and the required processing time was determined by both visually and  
162 quantitatively assessing model topographical variance. Datasets for modeling three human  
163 subjects were imported into Metashape where models were rendered using 120, 100, 90, 80, 60,  
164 40, 30, 20, and 10 photos and their processing times were recorded. Each model was exported as  
165 a '.obj' file into Meshmixer, scaled, and then exported into CloudCompare (CC), an open-source  
166 point cloud software, for displacement analysis. In CC, the facial models were aligned, cropped,  
167 and registered using the Iterative Closest Point (ICP) function. The models constructed from 120  
168 photos were used as a reference to compare models rendered models smaller subsets of the 120  
169 source photograph dataset for each subject. Model quality was both quantitatively and qualitatively  
170 evaluated by evaluating smoothness of the topographical appearance (qualitative) and and by  
171 analyzing the distribution of mesh face displacement compared to the reference models

172 (quantitative). Models with greater variance compared to reference models were deemed lower  
173 quality.

174

### 175 *Volumetric Analysis of Phantom Lesions*

176 To quantify the volumetric accuracy of the PHACE system, three 3D printed hemispheric  
177 phantom lesions of different sizes were affixed above the brow line to simulate facial lesions with  
178 known volumes. The phantom lesions were printed on a Prusa i3 MKS (Prusa Research, Prague,  
179 Czech Republic) 3D printer using Polylactic Acid (PLA) filament (Hatchbox, California, USA)  
180 with a layer resolution of 150 $\mu$ m. After printing, the surface texture was roughened using 2000  
181 grit sandpaper to reduce surface reflectivity. The volumes of the small, medium, and large phantom  
182 lesions were calculated using the volume formula for a hemisphere,  $\frac{2}{3}\pi\left(\frac{d}{2}\right)^3$ , where  $d$  was the  
183 diameter of the 3D printed hemisphere measured with a caliper at a resolution of 0.01mm  
184 (Mitutoyo digital caliper). Models of a face generated from images acquired with and without  
185 hemispheres attached to the face were exported from Metashape to CC where each model was  
186 manually aligned, and models were registered to each other. The paired models were then imported  
187 into Meshmixer where the models without hemispheres were Boolean subtracted from the models  
188 with phantom lesions. Each phantom lesion's volume was measured using Meshmixer's analysis  
189 stability tool and then compared with the manually calculated volume.

190

### 191 *Morphological Analysis in Anophthalmic Human Subject*

192 The PHACE system was further validated by comparing the depth displacement of the  
193 rendered model of the left orbit of an anophthalmic human subject to real world measurements  
194 using a Hertel exophthalmometer. The anophthalmic human subject was a male between 35-40

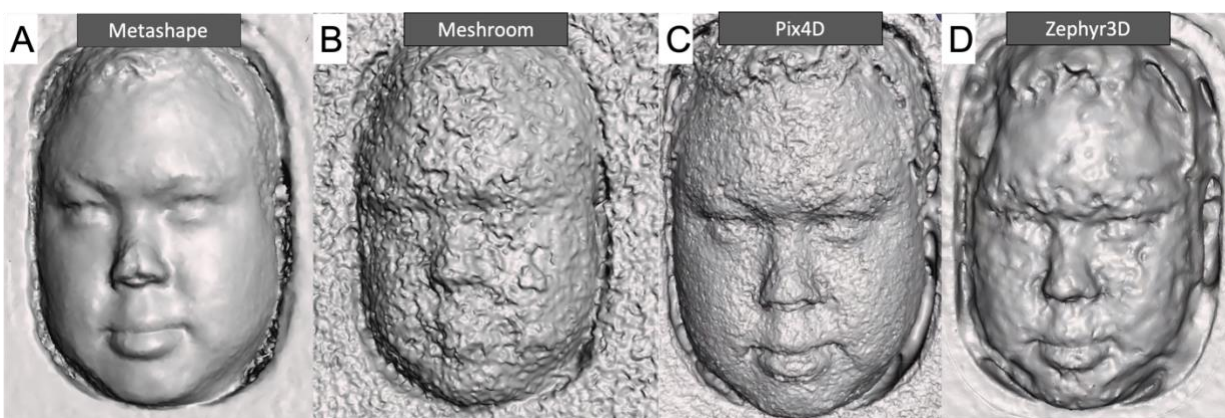
195 years-old with Fitzpatrick skin type 2 and a left ocular prosthetic. Models of the subject with and  
196 without the ocular prosthetic were rendered in Metashape, imported into CC, and registered to  
197 each other. A color map was calculated using orbital depth differences between mesh models with  
198 and without the ophthalmic prosthetic. The maximum depth displacement between the rendered  
199 facial models with and without the ocular prosthesis was compared to measurements made using  
200 the manual exophthalmometer.

201

## 202 Results

203 We compared models generated from four different photogrammetry software programs  
204 (Figure 2): Metashape (Agisoft, St. Petersburg, Russia), Meshroom (AliceVision), Pix4D (Prilly,  
205 Switzerland), and Zephyr3DLite (Verona, Italy) utilizing the highest setting for each software.  
206 Models generated using Metashape (Figure 2-A) qualitatively had the most facial normal-  
207 appearing facial features while minimizing excessive mesh surfaces that cause unwanted  
208 topographical textures or obscure subtle facial features (Figure 2 B-D).

209

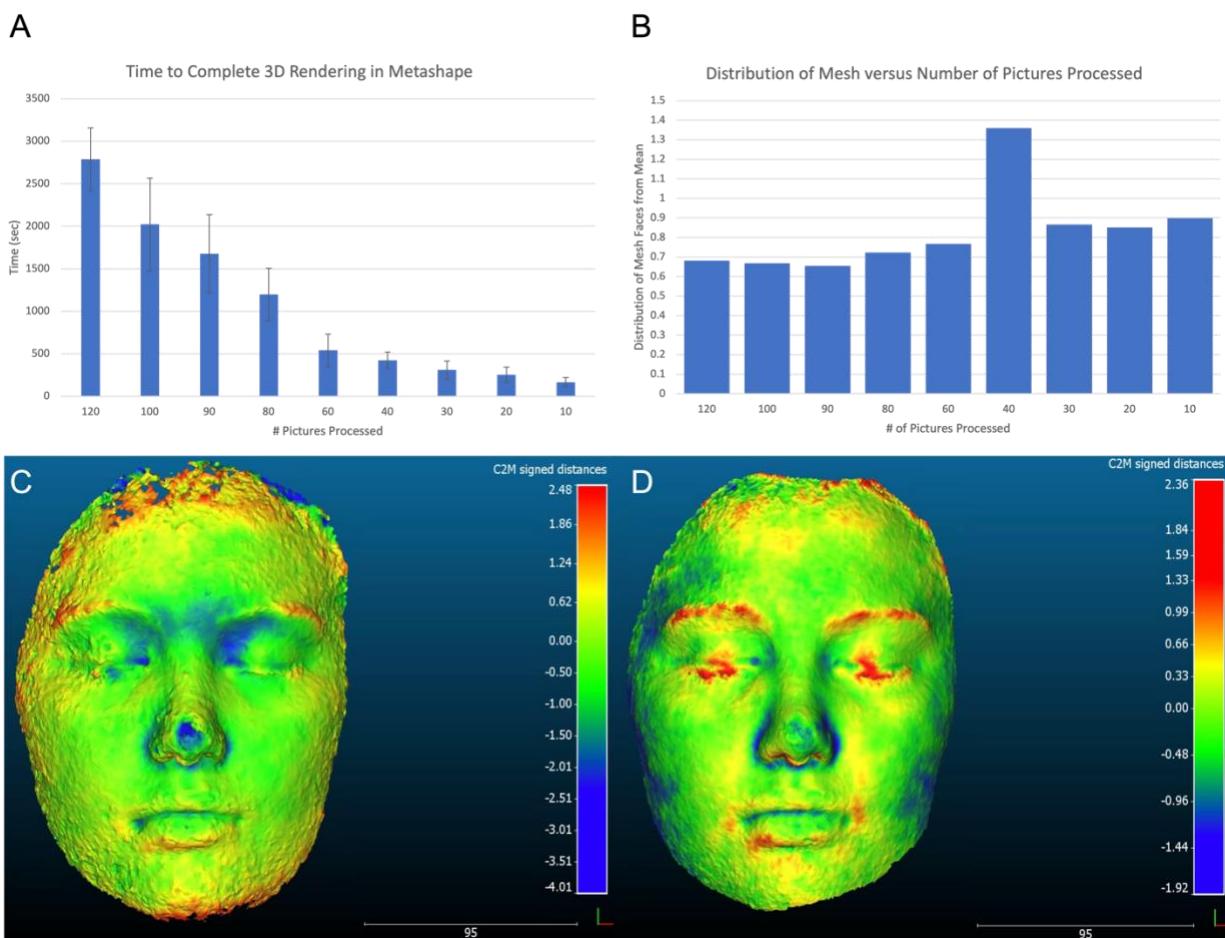


210

211

Figure 2. Comparison of four photogrammetry software packages to render facial models. The same photography dataset was used for Agisoft (A), Meshroom (B), Pix4D (C), and Zephyr3D (D).

212 Next, subsets of 10 to 120 photos were processed and compared using 3D mesh models in  
213 CC. It was found that at least 90 photos (25-minute processing time) were required to create a 3D  
214 model without compromising precision (Figure 3A – B). The facial model from 120 photos varied  
215 from -1.92mm to 2.36mm compared to the mean facial surface. The model in Figure 3D used 20  
216 photos and varied -4.01mm to 2.48mm.  
217






218 Figure 3. Average distribution of the mesh faces from the mean when using 10 to 120  
219 pictures (A). Average time to create a 3D model using 10 to 120 photos (B). Models  
220 generated using 20 (C) and 120 photographs (D).

221

222 The hemispheric phantom lesion volumes measured using Meshmixer to evaluate models  
223 produced by the PHACE system are shown in Table 2. The PHACE system yielded a 2.5% volume  
224 error (52.4 $\mu$ L) compared with the manually calculated reference volume of 2060 $\mu$ L for the large  
225 3D printed hemispherical phantom. A similar error of 2.5% was found for the medium sized  
226 (244 $\mu$ L) phantom. The smallest phantom demonstrated the greatest absolute error of 7.6% which  
227 accounted for a volumetric difference of 2.1 $\mu$ L.

228

229 **Table 2.** Manually calculated versus 3D digitally measured volume for the three phantom lesion  
230 sizes.

PHANTOM LESION DIAMETER (mm)	CALCULATED VOLUME ( $\mu$ L)	DIGITAL VOLUMETRIC ANALYSIS ( $\mu$ L)	ABSOLUTE MEAN DIFFERENCE ( $\mu$ L)	% DIFFERENCE
 19.89 $\pm$ 0.05	2060 $\pm$ 30	2112.4 $\pm$ 94.6	52.4	2.5 %
 9.78 $\pm$ 0.05	244 $\pm$ 8	238.7 $\pm$ 20.0	6.2	2.5 %
 4.72 $\pm$ 0.05	27.5 $\pm$ 2	25.4 $\pm$ 5.1	2.1	7.6 %

231

232

233 In the anophthalmic subject (Figure 4), the left eye depth without the ophthalmic prosthetic  
234 was measured with a Hertel exophthalmometer. The exophthalmometer quantified a difference  
235 3.5mm of lid protrusion with and without the prosthetic in place. PHACE measured a depth  
236 difference of 4.22mm (Figure 4).

237



Figure 4, Model depth analysis of human subject with ophthalmic prosthesis (top), without prosthesis (middle), and colorized depth map (bottom) representing differences in depth. The automated photogrammetry model with overlaying depth map shows a depth difference of -4.22 mm.

238

239

## 240 Discussion

241 3D anthropometry is a continuously evolving field as technology continues to improve.  
242 There are few studies and specific technologies that evaluate 3D periorbital anthropometry for  
243 clinical use. In this study, we optimized our PHACE system with focus on optimizing both low-  
244 cost components while maintaining topographical resolution to computationally reconstruct  
245 human faces for digital quantitative analysis. This study used free software and a novel volumetric  
246 methodology for depth analysis to characterize the PHACE system.

247

### 248 *Optimized Automated Stereophotogrammetry*

249 The PHACE system was developed with stereophotogrammetry at its core. Unlike high  
250 and mid-cost structured light scanning technologies, photogrammetry is the most ubiquitous,  
251 economical and versatile 3D modeling technique currently available. Any low-cost camera system

252 (e.g., a smartphone or raspberry pi camera) in combination with an affordable or open-source  
253 photogrammetry software can be used to safely and accurately render high quality models with  
254 potential utility in healthcare.

255 Although Murta et al. demonstrated the utility and clinical need for quantitative 3D  
256 methods of evaluating facial morphology in the setting of ocular disease/ophthalmic interventions  
257 (e.g., orbit decompression for thyroid eye disease) they use an expensive stereophotogrammetric  
258 system costing thousands of dollars.<sup>34</sup> There are no well-established or routinely employed  
259 affordable automated systems that produce high quality models for morphologic and volumetric  
260 evaluation in ophthalmology. The PHACE system uses off-the-shelf and 3D printed components  
261 to create an automated imaging system to reproducibly procure photographs of subject faces from  
262 multiple different angles with very little human input. Reconstructing 3D facial models for medical  
263 evaluation requires clear, high-resolution photographs to be able to discriminate millimeter and  
264 sub-millimeter sized features. Automated camera actuation and photograph acquisition remove  
265 interoperator variability, which is important in 3D model measuring reproducibility. Ceinos et al.  
266 found that there was minimal inter-examiner variability in obtaining facial measurements from  
267 stereophotogrammetry scans when scans are acquired manually<sup>35</sup>, and automating the process  
268 further reduces potential variability. Therefore, the PHACE system (Figure 1-A) is a clinically  
269 optimized, low-cost automated stereo-capture system using off-the-shelf components.

270 The photogrammetry software is equally important to the 3D model optimization. Not all  
271 photogrammetry software tools perform equally, and Figure 2 compares the quality of rendered  
272 models between different photogrammetry software using the same 100 photographs. Metashape  
273 reconstructs faces with the highest detail, while also minimizing the extraneous mesh noise (Figure  
274 2A). In contrast, the model constructed by Pix4D exhibits detailed facial features (i.e., the contour

275 of the eyelids and adnexa can be distinguished); however, the model has significant mesh noise  
276 that show an artificial surface texture and can obscure subtle surface detail (Figure 2C). Guo et al.  
277 established several landmarks that are useful in the analysis of periorbital anthropometric scans,  
278 including the medial canthus and lateral canthus, and upper and lower eyelid margin.<sup>35</sup> With  
279 significant mesh noise and artificial surface texture in Pix4D reconstructions, such important  
280 landmarks are indistinguishable, and thus not useful to track clinical progress over time. Both  
281 Meshroom and Zephyr3D create lower quality mesh models that are qualitatively unsuitable for  
282 clinical use (Figure 2B and 2D). Therefore, the PHACE protocol adopted Metashape  
283 photogrammetry software to reconstruct all facial models.

284 The final significant factor in optimizing model reconstruction is collecting an optimal  
285 number of images. When reducing the number of images processed, the time required to generate  
286 images is reduced (Figure 3A). This finding confirms Maas et al. who found that computational  
287 effort grows exponentially with the number of photos processed.<sup>36</sup> However, when reducing the  
288 number of images, the precision of the model is also reduced. With fewer photos, there is an  
289 increased distribution of mesh faces displaced from the surface of the face (Figure 3B). The  
290 comparison between the two sample facial reconstructions (Figure 3C and 3D) highlights the  
291 reduced model precision with fewer photos. Ultimately, we found that approximately 90 photos  
292 were required to create a 3D model without compromising precision.

293

#### 294 *Validation of Automated Stereophotogrammetry*

295 Two methods were used to validate our novel automated photogrammetry system:  
296 quantitative volumetric analysis of phantoms and exophthalmometry in a patient with an ocular  
297 prosthetic. Prior studies have only evaluated the dimensional accuracy by measuring displacement



298 of rendered models to a reference.<sup>38,39</sup> However, measuring differences in linear distance between  
299 rendered and reference models is limited to interpreting 3D volumetric changes from a 2D imaging  
300 plane. Therefore, we quantitatively measured volumes to objectively assess dimensional and  
301 morphological accuracy. Our novel methodology to assess digital facial reconstruction techniques  
302 used phantom lesions made of 3D printed hemispheres attached to the ocular adnexa to evaluate  
303 volumetric and dimensional accuracy. Therefore, we custom designed 3D printed hemispheric  
304 phantom to compare known volumes with volumes calculated from PHACE models. The results  
305 shown in Table 2 demonstrate that the automated photogrammetry system is able to measure an  
306 average volume as small as  $244\mu\text{L}^3$  with only a 2.5% difference. Because the double-sided tape  
307 attaching the hemispheres to the ocular adnexa is 0.1mm thick,  $7.5\mu\text{L}$  must be subtracted from the  
308 artificially increased, digitally measured volume of the hemisphere on the ocular adnexa.  
309 Therefore, the photogrammetry system was able to digitally quantify the  $244\mu\text{L}$  hemisphere with  
310 an accuracy of an average of  $238.7 \pm 20\mu\text{L}$ , which is a 2.5% error and less than the volume of  
311 uncertainty due to error propagation from the resolution accuracy of the digital calipers (6.6%).  
312 The  $27.5\mu\text{L}$  small hemisphere was reconstructed with an average accuracy of  $25.4 \pm 5.1\mu\text{L}$ , which  
313 is a 7.6% difference and greater than the error propagation due to the digital caliper resolution.  
314 Therefore, the PHACE system can accurately recapitulate small volumes to within 2.5 to 7.6%  
315 accuracy. This is more accurate than the published findings of 5-14 mL volume differences when  
316 measuring volumetric changes in facial swelling after orthognathic surgery using 3D  
317 stereophotogrammetry scans of the head and neck using the 3dMDface stereophotogrammetry  
318 system.<sup>40</sup>

319 Quantitative depth analysis was performed on rendered models from a human subject with  
320 and without his prosthetic eye and compared to measurements obtained via a Hertel

321 exophthalmometer (Figure 4). The change in depth digitally measured by the PHACE system was  
322 -4.22mm, while the exophthalmometer measured a change in depth of -3.5mm. However, the  
323 exophthalmometer's resolution is limited to millimeters and can only be subjectively estimated by  
324 in 0.5mm increments. Therefore, comparing digital depth measurements to human manual  
325 exophthalmometer measurements can easily suffer from subjective user variability. Experts in the  
326 field agree that measurements with the Hertel exophthalmometer are not exact but should be  
327 repeatable within 1-2mm.<sup>41</sup> Therefore, our measurements from the PHACE digital model fall  
328 within the standard error limits of the standard exophthalmometer measurement ability.

329

### 330 *Limitations and Future Directions*

331 A significant consideration when using a 3D model reconstruction technique for  
332 quantitative change analysis of human faces is that subtle micro-expressions will drastically reduce  
333 the comparability between models and ultimately lower the sensitivity of the analysis. In theory,  
334 after reconstructed models are registered to each other in 3D space, all changes detected are due  
335 to external factors altering the region of interest. In the medical context, changes between models  
336 will ideally be due solely to medical conditions altering tissue volume and depth. However, facial  
337 micro-expressions as simple as a subtle smile or frown will alter the 3D model. Brons et al. found  
338 that involuntary facial expressions can make significant differences in 3D images, particularly  
339 along the nasolabial region.<sup>42</sup> The error from involuntary facial expressions may propagate and  
340 amplify during model alignment and registration in 3D space. When reconstructed models are  
341 registered in 3D space, subtle changes to any model region can alter the alignment and registration  
342 of the models. To address this concern, we asked subjects to close their eyes and relax their faces.  
343 The effect of microexpression on open eyelid morphology will need to be investigated thoroughly

344 before systems like PHACE can reliably quantify changes in tissue volumes affecting eyelid  
345 morphology.

346 To procure reliable measurements on 3D rendered faces, visual landmarks consistent  
347 across varying human faces needs to be established. Several groups have investigated the breadth  
348 of periorbital anthropometric technologies available and have helped define standardized  
349 landmarks that can be used, including the medial canthus and lateral canthus, and upper and  
350 lower eyelid margins.<sup>36,43,44</sup> The implementation of standardized landmarks will help align  
351 photos more accurately and allow clinicians to make accurate measurements using digitally  
352 reconstructed models, and in turn to compare clinical changes over time. Future directions to  
353 make this technology more clinically useful including automating MeshMixer in such a manner  
354 so that clinicians can readily obtain image output measurements without engaging any lengthy  
355 imaging analysis protocols.

356

## 357 **Conclusions**

358 We optimized parameters for an automated stereophotogrammetry imaging system using  
359 a photogrammetric software protocol. We have also demonstrated a novel method for evaluating  
360 volumetric dimensional accuracy of 3D reconstruction techniques by comparing digitally  
361 measured volumes of 3D printed hemispheric phantom lesions against their calculated volumes.  
362 The PHACE system can accurately recapitulate volumes as small as 244 $\mu$ L to approximately  
363 2.5%. This affordable and easy-to-use stereophotogrammetry system should be considered in  
364 clinical settings to evaluate volumetric dynamics over the course of care.

365 **References**

- 366 1. Ey-Chmielewska H, Chruściel-Nogalska M, Frączak B. Photogrammetry and Its Potential  
367 Application in Medical Science on the Basis of Selected Literature. *Adv Clin Exp Med.*  
368 2015;24(4):737-741.
- 369 2. Pilgrim LJ. History of photogrammetry in medicine. *Australas Phys Eng Sci Med.*  
370 1992;15(1):1-8.
- 371 3. Bosemann W. Advances in photogrammetric measurement solutions. *Comput Ind.*  
372 2005;56(8-9):886-893.
- 373 4. Mitchell HL, Newton I. Medical photogrammetric measurement: overview and prospects.  
374 *ISPRS P&RS.* 2002;56(5-6):295–310.
- 375 5. Lussu P, Marini E. Ultra close-range digital photogrammetry in skeletal anthropology: A  
376 systematic review. *PLoS One.* 2020;15(4):e0230948.
- 377 6. Porto AB, Okazaki VHA. Procedures of assessment on the quantification of thoracic  
378 kyphosis and lumbar lordosis by radiography and photogrammetry: A literature review. *J*  
379 *Bodyw Mov Ther.* 2017;21(4):986-994.
- 380 7. Haleem A, Javaid M. 3D scanning applications in medical field: A literature-based  
381 review. *Clin. Epidemiol. Glob. Health.* 2019;7(2):199-210.
- 382 8. Kaderli A, Katircioglu Y, Ozdemir ES, Kaderli ST. Long-term comparison of the efficacies  
383 of internal and external browpexy combined with blepharoplasty. *Arq Bras Oftalmol.*  
384 2020;83(3):185-189.
- 385 9. Takamoto T, Schwartz B. Photogrammetric measurement of nerve fiber layer  
386 thickness. *Ophthalmology.* 1989;96(9):1315-1319.

- 387 10. Romano PE. Simple photogrammetric diagnosis of optic nerve hypoplasia. *Arch*  
388 *Ophthalmol.* 1989;107(6):824–826.
- 389 11. Azuara-Blanco A, Spaeth GL. Methods to objectify reversibility of glaucomatous  
390 cupping. *Curr Opin Ophthalmol.* 1997;8(2):50-54.
- 391 12. Knoops PG, Beaumont CA, Borghi A, et al. Comparison of three-dimensional scanner  
392 systems for craniomaxillofacial imaging. *J Plast Reconstr Aesthet Surg.* 2017;70(4):441-  
393 449.
- 394 13. Heike CL, Upson K, Stuhaug E, Weinberg SM. 3D digital stereophotogrammetry: a  
395 practical guide to facial image acquisition. *Head Face Med.* 2010;6:18.
- 396 14. Lekakis G, Claes P, Hamilton GS 3rd, Hellings PW. Three-Dimensional Surface Imaging  
397 and the Continuous Evolution of Preoperative and Postoperative Assessment in  
398 Rhinoplasty. *Facial Plast Surg.* 2016 Feb;32(1):88-94.
- 399 15. Struck R, Cordoni S, Aliotta S, Pérez-Pachón L, Gröning F. Application of  
400 Photogrammetry in Biomedical Science. *Adv Exp Med Biol.* 2019;1120:121-130.
- 401 16. Verhulst A, Hol M, Vreeken R, Becking A, Ulrich D, Maal T. Three-Dimensional Imaging  
402 of the Face: A Comparison Between Three Different Imaging Modalities. *Aesthet Surg J.*  
403 2018;38(6):579-585.
- 404 17. Hong C, Choi K, Kachroo Y, et al. Evaluation of the 3dMDface system as a tool for soft  
405 tissue analysis. *Orthod Craniofac Res.* 2017;20 Suppl 1(Suppl 1):119-124.
- 406 18. Nord F, Ferjencik R, Seifert B, et al. The 3dMD photogrammetric photo system in cranio-  
407 maxillofacial surgery: Validation of interexaminer variations and perceptions. *J*  
408 *Cranio-maxillofac Surg.* 2015;43(9):1798-1803.

- 409 19. Dindaroğlu F, Kutlu P, Duran GS, Görgülü S, Aslan E. Accuracy and reliability of 3D  
410 stereophotogrammetry: A comparison to direct anthropometry and 2D  
411 photogrammetry. *Angle Orthod*. 2016;86(3):487-494.
- 412 20. Tzou CH, Artner NM, Pona I, et al. Comparison of three-dimensional surface-imaging  
413 systems. *J Plast Reconstr Aesthet Surg*. 2014;67(4):489-497.
- 414 21. Camison L, Bykowski M, Lee WW, et al. Validation of the Vectra H1 portable three-  
415 dimensional photogrammetry system for facial imaging. *Int J Oral Maxillofac Surg*.  
416 2018;47(3):403-410.
- 417 22. Gibelli D, Pucciarelli V, Cappella A, Dolci C, Sforza C. Are Portable  
418 Stereophotogrammetric Devices Reliable in Facial Imaging? A Validation Study of  
419 VECTRA H1 Device. *J Oral Maxillofac Surg*. 2018;76(8):1772-1784.
- 420 23. Savoldelli C, Benat G, Castillo L, Chamorey E, Lutz JC. Accuracy, repeatability and  
421 reproducibility of a handheld three-dimensional facial imaging device: The Vectra H1. *J*  
422 *Stomatol Oral Maxillofac Surg*. 2019;120(4):289-296.
- 423 24. Ritschl LM, Roth M, Fichter AM, et al. The possibilities of a portable low-budget three-  
424 dimensional stereophotogrammetry system in neonates: a prospective growth analysis and  
425 analysis of accuracy. *Head Face Med*. 2018;14(1):11.
- 426 25. Rudy HL, Wake N, Yee J, Garfein ES, Tepper OM. Three-Dimensional Facial Scanning  
427 at the Fingertips of Patients and Surgeons: Accuracy and Precision Testing of iPhone X  
428 Three-Dimensional Scanner. *Plast Reconstr Surg*. 2020;146(6):1407-1417.
- 429 26. Products. 3dMD. Accessed 22February 14, 2023. <https://3dmd.com/products/>
- 430 27. Vectra H2. Canfield Care. Accessed February 14, 2023.  
431 <https://www.canfieldsci.com/imaging-systems/vectra-h2-3d-imaging-system/>

- 432 28. Artec Eva. Artec 3D. Accessed February 14, 2023. [https://www.artec3d.com/portable-3d-](https://www.artec3d.com/portable-3d-scanners/artec-eva)  
433 [scanners/artec-eva](https://www.artec3d.com/portable-3d-scanners/artec-eva)
- 434 29. Breitbarth A, Schardt T, Kind C, Brinkmann J, Dittrich PG, Notni G. Measurement  
435 accuracy and dependence on external influences of the iPhone X TrueDepth sensor.  
436 Photonics and Education in Measurement Science. 2019. Proc. SPIE 11144. doi  
437 10.1117/12.2530544
- 438 30. Jayaratne YS, Deutsch CK, Zwahlen RA. Normative findings for periocular  
439 anthropometric measurements among Chinese young adults in Hong Kong. *Biomed Res*  
440 *Int.* 2013;2013:821428.
- 441 31. Guo Y, Rokohl AC, Schaub F, Hou X, Liu J, Ruan Y, Jia R, Koch KR, Heindl LM.  
442 Reliability of periocular anthropometry using three-dimensional digital  
443 stereophotogrammetry. *Graefes Arch Clin Exp Ophthalmol.* 2019 Nov;257(11):2517-  
444 2531.
- 445 32. Liu J, Guo Y, Arakelyan M, Rokohl AC, Heindl LM. Accuracy of Areal Measurement in  
446 the Periocular Region Using Stereophotogrammetry [published online ahead of print, 2020  
447 Dec 17]. *J Oral Maxillofac Surg.* 2020;S0278-2391(20)31512-3.
- 448 33. Hyer JN, Murta F, Juniat VAR, Ezra DG. Validating three-dimensional imaging for  
449 volumetric assessment of periorbital soft tissue. *Orbit.* 2021;40(1):9-17.
- 450 34. Murta, Fabiola, et al. "Quantitative assessment of orbital decompression surgery using  
451 Photogrammetric Stereoimaging." *Ophthalmic Plastic and Reconstructive Surgery* 37.5  
452 (2021): 420-423.

- 453 35. Ceinos R, Tardivo D, Bertrand MF, Lupi-Pegurier L. Inter- and Intra-Operator Reliability  
454 of Facial and Dental Measurements Using 3D-Stereophotogrammetry. *J Esthet Restor*  
455 *Dent.* 2016;28(3):178-189. doi:10.1111/jerd.12194
- 456 36. Guo, Y, Rokohl, AC, Lin, M, Heindl, LM. "Three-dimensional anthropometry in  
457 periorbital region." *Ann Eye Sci* 6.8 (2020): 10-21037.
- 458 37. Maas HG. Concepts of real-time photogrammetry. *Human Movement Science.* 1997;16(2-  
459 3):189-199. doi:10.1016/S0167-9457(96)00049-8
- 460 38. Mao B, Li J, Tian Y, Zhou Y. The accuracy of a three-dimensional face model  
461 reconstructing method based on conventional clinical two-dimensional photos. *BMC Oral*  
462 *Health.* 2022 Sep 19;22(1):413. doi: 10.1186/s12903-022-02439-0. PMID: 36123646;  
463 PMCID: PMC9487071.
- 464 39. Pan F, Liu J, Cen Y, et al. Accuracy of RGB-D camera-based and stereophotogrammetric  
465 facial scanners: a comparative study. *J Dent.* 2022;127:104302.  
466 doi:10.1016/j.jdent.2022.104302
- 467 40. Buitenhuis MB, Klijn RJ, Rosenberg AJWP, Speksnijder CM. Reliability of 3D  
468 Stereophotogrammetry for Measuring Postoperative Facial Swelling. *J Clin Med.*  
469 2022;11(23):7137. Published 2022 Nov 30. doi:10.3390/jcm11237137
- 470 41. Nerad JA. Diagnostic Approach to the Patient with Proptosis. In: Nerad JA, ed. *Techniques*  
471 *in Ophthalmic Plastic Surgery (Second Edition).* Elsevier; 2021:545-610. doi  
472 10.1016/B978-0-323-39316-4.00014-4
- 473 42. Brons S, Darroudi A, Nada R, et al. Influence of involuntary facial expressions on  
474 reproducibility of 3D stereophotogrammetry in children with and without complete



- 475 unilateral cleft lip and palate from 3 to 18 months of age. Clin Oral Investig.  
476 2019;23(3):1041-1050. doi:10.1007/s00784-018-2520-0
- 477 43. Gibelli D, Pucciarelli V, Poppa P, et al. Three-dimensional facial anatomy evaluation:  
478 Reliability of laser scanner consecutive scans procedure in comparison with  
479 stereophotogrammetry. J Craniomaxillofac Surg 2018;46:1807-13.
- 480 44. Li Q, Zhang X, Li K, et al. Normative anthropometric analysis and aesthetic indication of  
481 the ocular region for young Chinese adults. Graefes Arch Clin Exp Ophthalmol  
482 2016;254:189-97.